Published OnlineFirst February 12, 2018; DOI: 10.1158/0008-5472.CAN-17-2726

Molecular Cell Biology

Cancer Research

Oncogenic Kinase–Induced PKM2 Tyrosine 105 Phosphorylation Converts Nononcogenic PKM2 to a Tumor Promoter and Induces Cancer Stem–like Cells

Zhifen Zhou[1,2], Min Li[2], Lin Zhang[2,3], Hong Zhao[2], Özgür Şahin[2], Jing Chen[4], Jean J. Zhao[5], Zhou Songyang[1,6], and Dihua Yu[2,3,7]

Abstract

The role of pyruvate kinase M2 isoform (PKM2) in tumor progression has been controversial. Previous studies showed that PKM2 promoted tumor growth in xenograft models; however, depletion of PKM2 in the *Brca1*-loss–driven mammary tumor mouse model accelerates tumor formation. Because oncogenic kinases are frequently activated in tumors and PKM2 phosphorylation promotes tumor growth, we hypothesized that phosphorylation of PKM2 by activated kinases in tumor cells confers PKM2 oncogenic function, whereas nonphosphorylated PKM2 is nononcogenic. Indeed, PKM2 was phosphorylated at tyrosine 105 (Y105) and formed oncogenic dimers in MDA-MB-231 breast cancer cells, whereas PKM2 was largely unphosphorylated and formed nontumorigenic tetramers in nontransformed MCF10A cells. PKM2 knockdown did not affect MCF10A cell growth but significantly decreased proliferation of MDA-MB-231 breast cancer cells with tyrosine kinase activation. Multiple kinases that are frequently activated in different cancer types were identified to phosphorylate PKM2-Y105 in our tyrosine kinase screening. Introduction of the PKM2-Y105D phosphomimetic mutant into MCF10A cells induced colony formation and the $CD44^{hi}/CD24^{neg}$ cancer stem–like cell population by increasing Yes-associated protein (YAP) nuclear localization. ErbB2, a strong inducer of PKM2-Y105 phosphorylation, boosted nuclear localization of YAP and enhanced the cancer stem–like cell population. Treatment with the ErbB2 kinase inhibitor lapatinib decreased PKM2-Y105 phosphorylation and cancer stem–like cells, impeding PKM2 tumor-promoting function. Taken together, phosphorylation of PKM2-Y105 by activated kinases exerts oncogenic functions in part via activation of YAP downstream signaling to increase cancer stem–like cell properties.

Significance: These findings reveal PKM2 promotes tumorigenesis by inducing cancer stem-like cell properties and clarify the paradox of PKM2's dichotomous functions in tumor progression. *Cancer Res; 78(9); 2248–61. ©2018 AACR.*

Introduction

PKM2 is the M2 isoform of pyruvate kinase (PK), catalyzing pyruvate and adenosine 5′-triphosphate (ATP) production by transferring the phosphate from phosphoenolpyruvate (PEP) to adenosine 5′-diphosphate (ADP; ref. 1). Among the PK genes in mammals, the *PKM* gene encodes PKM1 and PKM2 isoforms by the mutually exclusive use of exons 9 and 10 (2). PKM2 has lower PK activity than PKM1, but PKM2 can be allosterically activated by its upstream metabolite fructose-1, 6-bisphosphate (FBP; refs. 3, 4). PKM1 is mainly expressed in the heart, muscle, and brain, whereas PKM2 is expressed in less differentiated, highly proliferating tissues, such as early fetal tissues, intestines, and especially most tumors (5).

PKM2 has been shown to promote tumor growth by inhibiting apoptosis in tumor cells (6) or switching cancer metabolism to aerobic glycolysis and channeling nutrients into biosynthesis (7, 8). PKM2 also has oncogenic functions that are independent of its role in glycolysis. For example, upon EGFR activation, Erk1/2-dependent phosphorylation of PKM2 at serine 37 (S37) promotes PKM2 translocation, which activates β-catenin to promote U87 glioma tumor cell proliferation and tumorigenesis (9–11). However, the role of PKM2 in tumor progression is complex and controversial. PKM2 deletion in the mammary glands of a *Brca1*-loss–driven tumor model did not postpone tumorigenesis (12). In addition, mice with germline loss of *Pkm2* developed hepatocellular carcinoma earlier compared with the age-matched wild-type (WT) mice (13). Data from these two studies indicated that PKM2 is tumor suppressive in nontransformed mouse tissues. Clearly, PKM2 has opposing functions in nontransformed tissues versus in tumor tissues. It is unknown how and when PKM2 gains the oncogenic function during tumorigenesis.

[1]Key Laboratory of Gene Engineering of the Ministry of Education, State Key Laboratory of Oncology in South China, Institute of Healthy Aging Research, School of Life Sciences, Sun Yat-sen University, Guangzhou, China. [2]Department of Molecular and Cellular Oncology, The University of Texas MD Anderson Cancer Center, Houston, Texas. [3]MD Anderson Cancer Center UTHealth Graduate School of Biomedical Sciences, Houston, Texas. [4]Winship Cancer Institute, Emory University School of Medicine, Atlanta, Georgia. [5]Department of Biological Chemistry and Molecular Pharmacology, Harvard Medical School, Boston, Massachusetts. [6]Verna and Marrs McLean Department of Biochemistry and Molecular Biology, Baylor College of Medicine, Houston, Texas. [7]Center for Molecular Medicine, China Medical University, Taichung, Taiwan.

Note: Supplementary data for this article are available at Cancer Research Online (http://cancerres.aacrjournals.org/).

Z. Zhou, M. Li, and L. Zhang contributed equally to this article.

Corresponding Author: Dihua Yu, The University of Texas MD Anderson Cancer Center, Houston, 1515 Holcombe Boulevard, TX 77054. Phone: 713-792-3636; Fax: 713-792-4544; E-mail: dyu@mdanderson.org

doi: 10.1158/0008-5472.CAN-17-2726

Published OnlineFirst February 12, 2018; DOI: 10.1158/0008-5472.CAN-17-2726

Aberrant activation of oncogenic kinases, especially tyrosine kinases, is common during tumorigenesis (14, 15). Given that tyrosine phosphorylation of PKM2 promotes tumor growth (16, 17), we hypothesized that PKM2 gains distinct tumor-promoting functions owing to its posttranslational modification by oncogenic tyrosine kinases, which are activated in tumor tissues, but not in normal tissues. Indeed, we found that in breast cancer cells, PKM2 was phosphorylated by multiple tyrosine kinases, and formed dimers that promoted cancer cell growth, whereas, in nontransformed mammary epithelial cells, PKM2 was unphosphorylated and formed tetramers, which were dispensable for cell proliferation. We performed a tyrosine kinase screening and identified multiple tyrosine kinases that phosphorylated PKM2 at Y105 and promoted cell transformation. Phosphorylation of PKM2-Y105 induced cancer stem–like cell properties by enhancing Yes-associated protein (YAP) nuclear translocation. Inhibition of PKM2-Y105 phosphorylation by targeting ErbB2, a tyrosine kinase for PKM2-Y105, effectively reduced YAP nuclear translocation and cancer stem–like cells, and inhibited tumor growth. These data indicate that tyrosine phosphorylation of PKM2 by aberrantly activated kinases instigates oncogenic function of PKM2 during tumorigenesis.

Materials and Methods

Reagents and plasmids

Antibodies to phospho-PKM2-Tyrosine (Y) 105 (3827), PKM2 (4053), Flag M2 (14793), Met (3127), Tyro3 (5585), HER2/ErbB2 (2165), phospho-HER2/ErbB2 (Y1221/1222) (2243), FAK (3285), E-cadherin (14472), vimentin (5741), N-cadherin (13116), YAP (14074), phospho-YAP (Ser127) (4911), LATS1 (9153), and phospho-LATS1 (Ser909) (9157) were purchased from Cell Signaling Technology. Antibodies against ALDH (611194), FITC mouse anti-human CD44 (555478), FITC mouse IgG2b (555057), PE mouse anti-human CD24 (555428), and PE mouse IgG2a (554648) were from BD Biosciences. Lamin A/C antibody (sc-6215) and mounting medium with DAPI (sc-24941) were from Santa Cruz Biotechnology. Alexa Fluor 488 goat anti-rabbit (A11008) and Alexa Fluor 594 goat anti-mouse (A11005) secondary antibodies and the horseradish peroxidase (HRP)–linked antibodies against mouse (31430) and rabbit (31460) were from Thermo Fisher Scientific. Anti-mouse/human CD44 antibodies (103001) were purchased from BioLegend. Paraformaldehyde (PFA; 158127), PhosSTOP (4906837001), protease inhibitor cocktail (P8340), verteporfin (VP; SML0534), Protoporphyrin IX disodium salt (PPIX; 258385), β-actin antibody (A5441), and α-tubulin antibody (T6074) were from Sigma-Aldrich.

The kinase library was kindly provided by Dr. Jean Zhao's laboratory (18). The constructs expressing kinases AXL (23945), EPHA2 (23926), FAK (23902), MET (23889), and TYRO3 (23916) in the pDONR223 vector were purchased from Addgene, and these genes were transferred into pLentiN (37444) vector by Gateway cloning. pLHCX vector, pLHCX-Flag-mPKM2, and pLHCX-Flag-mPKM2-Y105F plasmids were from Dr. Jing Chen's laboratory (17). The mPKM2-Y105D mutation was induced using a Q5 Site-Directed Mutagenesis Kit (NEB, E0554S), and the primers were mPKM2-Y105D FP, 5′-GACCCCATCCTCGACCGGCCCGTTG-3′ and mPKM2-Y105D RP, 5′-CAACGGGCCGGTCGAGGATGGGGTC-3′. Flag-hPKM2 was cloned into pLHCX vector using HpaI and ClaI digestion. The primers were HpaI-Flag-hPKM2 FP, 5′-GTTAACGACTACAAAGACGATGACGACAAGATGTCGAAGCCCCATAGTG-3′, and ClaI-hPKM2 RP, 5′-ATCGATTCACGGCACAGGAACAAC-3′. The primers for hPKM2-Y105F mutations were hPKM2-Y105F FP, 5′-CCTCTTCCGGCCCGTTGCTGTGG-3′, and hPKM2 YF QC RP, 5′-GCCGGAAGAGGATGGGGTCAGAAGC-3′. The primers for hPKM2-Y105D mutations were hPKM2-Y105D FP, 5′-TCCTCGACCGGCCCGTTGCTGTG-3′, and hPKM2-Y105D RP, CCGGTCGAGGATGGGGTCAGAAGC.

Cell lines and cell culture

Human cell lines (MCF10A, MCF12A, MCF7, HCC1954, MDA-MB-361, BT474, MDA-MB-231, Hs578T, and MDA-MB-435) were purchased from ATCC and further characterized by the MD Anderson Cancer Center (MDACC) Characterized Cell Line Core Facility. All cell lines had been tested for *Mycoplasma* contamination. MCF10A and MCF12A cells were cultured in DMEM/F12 (Caisson DFL13) supplied with 5% horse serum (Thermo Fisher Scientific; 16050122), 20 ng/mL EGF, 0.5 μg/mL hydrocortisone, 100 ng/mL cholera toxin, 10 μg/mL insulin, and 1x penicillin/streptomycin solution (Invitrogen; 15070063) as previously described (19). Other cancer cells were cultured in DMEM/F12 supplied with 10% FBS (Thermo Fisher Scientific; SH3007103).

RNA interference and stable cell line generation

The shRNAs were cloned into pLKO.1 vector (Addgene; 10878). The target sequences were shPKM2-1, 5′-CTACCACTTGCAATTATTTGA-3′; shPKM2-2, 5′-CCACTTGCAATTATTTGAGGA-3′; shYAP1-1, 5′-TTGGTTGATAGTATCACCTGT-3′; and shYAP1-2, 5′-TTAAGGAAAGGATCTGAGCTA-3′. The shRNA gene knockdown or open reading frame gene expression lentiviral vectors were transfected into 293T cells together with packaging plasmid (psPAX2) and envelope plasmid (pMD2G) using the LipoD293 reagent (SignaGen; SL100668) according to the manufacturer's instructions. After 48 hours, the viruses were collected, filtered, and used to infect target cells in the presence of 8 to 10 μg/mL polybrene for 24 hours. The infected cells were selected by 250 μg/mL Hygromycin B Gold (InvivoGen; 31282-04-9) for 7 days or 2 μg/mL puromycin (InvivoGen; 58-58-2) for 3 days based on the drug selection genes of the introduced vectors.

Fractionation of cytoplasmic and nuclear proteins

In brief, cells were collected, resuspended in hypotonic buffer [10 mmol/L HEPES (pH 8.0), 1.5 mmol/L $MgCl_2$, and 10 mmol/L KCl], and incubated on ice for 15 minutes. They were then pelleted by centrifugation at 10,000 rpm at 4°C for 5 minutes. The pellet was resuspended in cytoplasm lysis buffer (hypotonic buffer + 0.5% NP-40) and incubated on ice for 30 minutes. Extracts were centrifuged at 13,000 rpm at 4°C for 10 minutes, and the supernatant was retained for the cytoplasmic fraction. The nuclear pellet was washed twice with hypotonic buffer and repelleted, and then resuspended in nuclear lysis buffer [10 mmol/L HEPES (pH 8.0), 1.5 mmol/L $MgCl_2$, 400 mmol/L NaCl, 0.1 mmol/L EDTA, and 20% glycerol], followed by incubation on ice for 30 minutes. A 30-gauge syringe was used to break up the pellet and release the nuclear proteins. Extracts were centrifuged at 13,000 rpm at 4°C for 15 minutes, and the supernatant was retained as the nuclear fraction.

Published OnlineFirst February 12, 2018; DOI: 10.1158/0008-5472.CAN-17-2726

Protein cross-linking and Western blot analysis

For protein cross-linking, 10^6 cells were collected, washed with PBS, and resuspended in 200 μL of 1% PFA in PBS for 7 minutes at room temperature, and the reaction was quenched with 800 μL of 125 mmol/L glycine in PBS for 5 minutes. Then, cells were lysed with Tris-free RIPA buffer (50 mmol/L HEPES, 150 mmol/L NaCl, 1 mmol/L EDTA, 1% NP-40, 0.1% SDS, adjust pH 7.4; proteinase inhibitor cocktail and phosphatase inhibitors were added before use) on ice for 30 minutes. The cells were centrifuged at 12,000 × *g* for 10 minutes, and the lysates were collected for Western blot analysis (20).

Flow cytometry analysis

Cells were seeded at the same density and collected when they reached 80% to 90% confluence. A million cells for each sample were washed twice in FACS buffer (1% BSA in PBS), resuspended in 100 μL FACS buffer, and then stained with 20 μL FITC mouse anti-human CD44 and PE mouse anti-human CD24 antibodies (BD Biosciences) or FITC mouse IgG2b and PE mouse IgG2a isotype controls on ice for 1 hour. Cells were washed with cold PBS twice and analyzed by FACSCanto II flow cytometer.

Immunofluorescence staining and confocal microscopy

Immunofluorescence staining and confocal microscopy were performed as previously described (21). Briefly, cells were fixed by 4% PFA, permeabilized with 0.3% TritonX-100, and blocked with 10% horse serum blocking buffer. Then the samples were incubated with Flag antibody (rabbit, 1:400 dilution) and/or YAP antibody (mouse, 1:100 dilution) at 4°C O/N, followed by staining with Alexa Fluor 488 Goat anti-Rabbit IgG and Alexa Fluor 594 Goat anti-Mouse IgG (1:500 dilution; Invitrogen). After mounting the slides with medium-containing DAPI, cells were visualized under a confocal laser scanning microscope (ZEISS LSM 880).

Quantitative real-time PCR

Total RNA was isolated using TRIzol reagent (Thermo Fisher Scientific; 15596026), and then reverse transcribed using the iScript cDNA Synthesis Kit (Bio-Rad; 1708891). To quantify gene expression, real-time PCR was conducted using SYBR FAST Universal qPCR Master Mix (Kapa Biosystems; KK4602) on a StepOnePlus real-time PCR system (Applied Biosystems). The relative expression of mRNAs was quantified by $2^{-\Delta\Delta Ct}$ with logarithm transformation. The following primers were used to detect corresponding mRNAs in the qRT-PCR analyses: CTGF FQP, 5′-TCGCCTTCGTGGTCCTCC-3′; CTGF RQP, 5′-GCCGAAGTCACAGAAGAGGC-3′; Cyr61 FQP, 5′-CTCGCCTTAGTCGTCACCC-3′; Cyr61 RQP, 5′-CGCCGAAGTTGCATTCCAG-3′; YAP1 FQP, 5′-TAGCCCTGCGTAGCCAGTTA-3′; YAP1 RQP, 5′-CTCATGCTTAGTCCACTGTCTGTAC-3′; LATS1 FQP, 5′-AATTTGGGACGCATCATAAAGC-3′; LATS1 RQP, 5′-TCGTCGAGGATCTTGGTAACTC-3′; 18S FQP, 5′-AACCCGTTGAACCCCATT-3′; and 18S RQP, 5′-CCATCCAATCGGTAGTAGCG-3′.

Cell proliferation assays

Cell proliferation was measured by the MTT assay as previously described (22). One thousand cells were seeded per well (six wells per sample) in 96-well plate, and the cell growth was examined by staining with MTT [3-(4,5-dimethylthiazol-2-yl)-2,5-diphenyltetrazolium bromide; Thermo Fisher Scientific; M6496]. The resulting intracellular purple formazan was solubilized by DMSO and analyzed for the OD570-OD650 using Gen5 Microplate reader (BioTek, Inc.).

Soft-agar colony formation assay

A soft-agar assay was performed as previously described (20). In brief, 0.5 mL of 0.6% agar containing 1× culture medium was added to each well of a 24-well plate. After the bottom agar was solidified, 0.5 mL of a mixture of 0.3% agar and 2,000 cells in 1× culture medium around 42°C was added on top of the 0.6% agar. One hundred microliters of medium were added twice weekly to prevent desiccation of the upper layer of agar. After 3 weeks, colonies were counted under the microscope.

Tyrosine kinases screening

The array of the kinases' antibodies was purchased from Cell Signaling Technology (#7982) for the kinase array screening. We modified the experimental procedures as follows: (i) 150 μg of cell lysates from MDA-MB-231 and MCF10A cells was added to the antibody arrays separately and incubated at 4°C O/N; (ii) purified Flag-PKM2 proteins from these two cell lines were added to the array that had been incubated with corresponding cell lysates and incubated at room temperature for 2 hours; (iii) Flag antibody conjugated with HRP was added for detecting the kinase–PKM2 interacting complexes; and (iv) the arrays were washed and developed with HRP substrate following the manufacturer's procedures. For the complementary mini-screening of additional kinases, tyrosine kinase constructs from the kinase library provided by Dr. Jean Zhao (18) were introduced into 293T cells.

Metabolic assays

To measure the glucose uptake (G), cells were starved for 3 hours before treatment with 100 μmol/L 2-NBDG (Sigma-Aldrich; 72987) for 30 minutes. Then the glucose uptake rate was analyzed by flow cytometry. For lactate production (L) measurement, cells were incubated in complete medium for 24 hours and tested by Accutrend lactate system (Roche). Oxygen consumption (O) was measured by Agilent Seahorse XF96 analyzer according to the manufacturer's instructions. Glycolysis index was calculated as previously reported (23).

Transgenic mouse model and treatment

All animal experiments and terminal endpoints were carried out in accordance with approved protocols from the Institutional Animal Care and Use Committee of MDACC. MMTV-NIC (Neu-IRES-Cre) mice were interbred with $PTEN^{fl/fl}$ mice to generate ErbB2/neu-overexpressing and PTEN homozygous loss ($PTEN^{-/-}$/NIC) mice (24). $PTEN^{-/-}$/NIC mice were randomized to each treatment group when their palpable tumors were 3 to 5 mm in diameter. Mice ($n = 5$ in each group) were treated daily with vehicle solution (0.5% wt/vol hydroxylpropyl-methyl-cellulose with 0.1% vol/vol Tween-20) or with lapatinib (LC Laboratories) at 100 mg/kg in vehicle solution via oral gavage for 3 weeks. Tumor growth was measured by caliper every 5 days. The mice were sacrificed after treatment, whereas tumors were harvested, weighted, and fixed for IHC staining. Normal mammary fat pad (MFP) tissues were from 10-week WT FVB mice.

IHC staining and score system

IHC staining was performed as previously described (20). Negative control slides without primary antibodies and positive

Published OnlineFirst February 12, 2018; DOI: 10.1158/0008-5472.CAN-17-2726

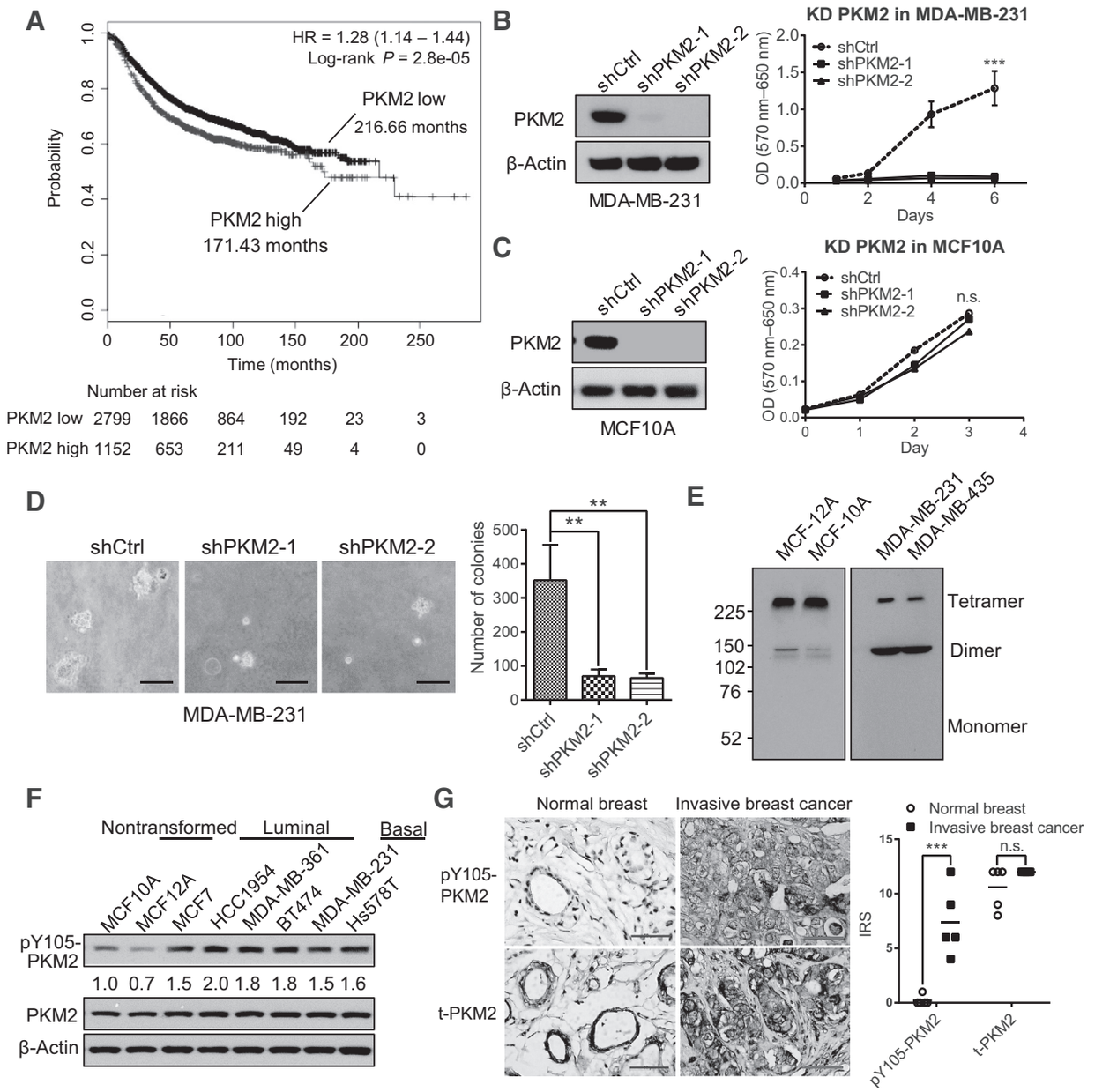

Figure 1.

PKM2 is essential for proliferation/transformation and is highly phosphorylated at Y105 in breast cancer cells. **A,** Kaplan–Meier survival curves of 3,951 patients with breast cancer whose tumors had a high or low PKM2 expression. **B,** Left, Western blot analysis of PKM2 expression in MDA-MB-231 cells transfected with control shRNA (shCtrl) or two different shRNAs against PKM2 (shPKM2-1 and shPKM2-2). Right, the growth curves of the indicated MDA-MB-231 sublines by MTT assays. ***, $P < 0.001$. **C,** Left, Western blot analysis of PKM2 expression in MCF10A cells transfected with shCtrl, shPKM2-1, or shPKM2-2. Right, the growth curves of the indicated MCF10A sublines by MTT assays. n.s., not statistically significant. **D,** Representative images (left) and quantification (right) of colony formation in soft agar from the PKM2 shRNA knockdown MDA-MB-231 sublines. **E,** Western blot analysis using PKM2 antibodies to detect PKM2 tetramers and dimers in nontransformed mammary epithelial cell lines (MCF-12A and MCF-10A) and in triple-negative breast cancer cell lines (MDA-MB-231 and MDA-MB-435). **F,** Western blot analysis of pY105-PKM2 and total PKM2 protein levels in the indicated nontransformed mammary epithelial cell lines versus luminal- and basal-type breast cancer cell lines. Quantification of pY105-PKM2 level in different cell lines compared with that in MCF10A (normalized to β-actin) was conducted by Image J software. **G,** Left, Representative IHC staining of pY105-PKM2 and total PKM2 proteins in human normal breast tissues versus in human invasive breast cancer samples. Right, quantification of the IRS of pY105 PKM2 and total PKM2 IHC staining in mammary epithelial cells of normal human breast and breast cancer samples ($n = 5$ in each group). ***, $P < 0.001$; n.s., not statistically significant.

control tissue slides were included for each staining. The immunoreactive score (IRS) was used to quantify the IHC staining, giving a range of 0 to 12 as a result of multiplication of positive cell proportion scores (0–4) and staining intensity scores (0–3) as previously reported (25). IHC staining and statistical analyses were performed in a double-blind manner.

Published OnlineFirst February 12, 2018; DOI: 10.1158/0008-5472.CAN-17-2726

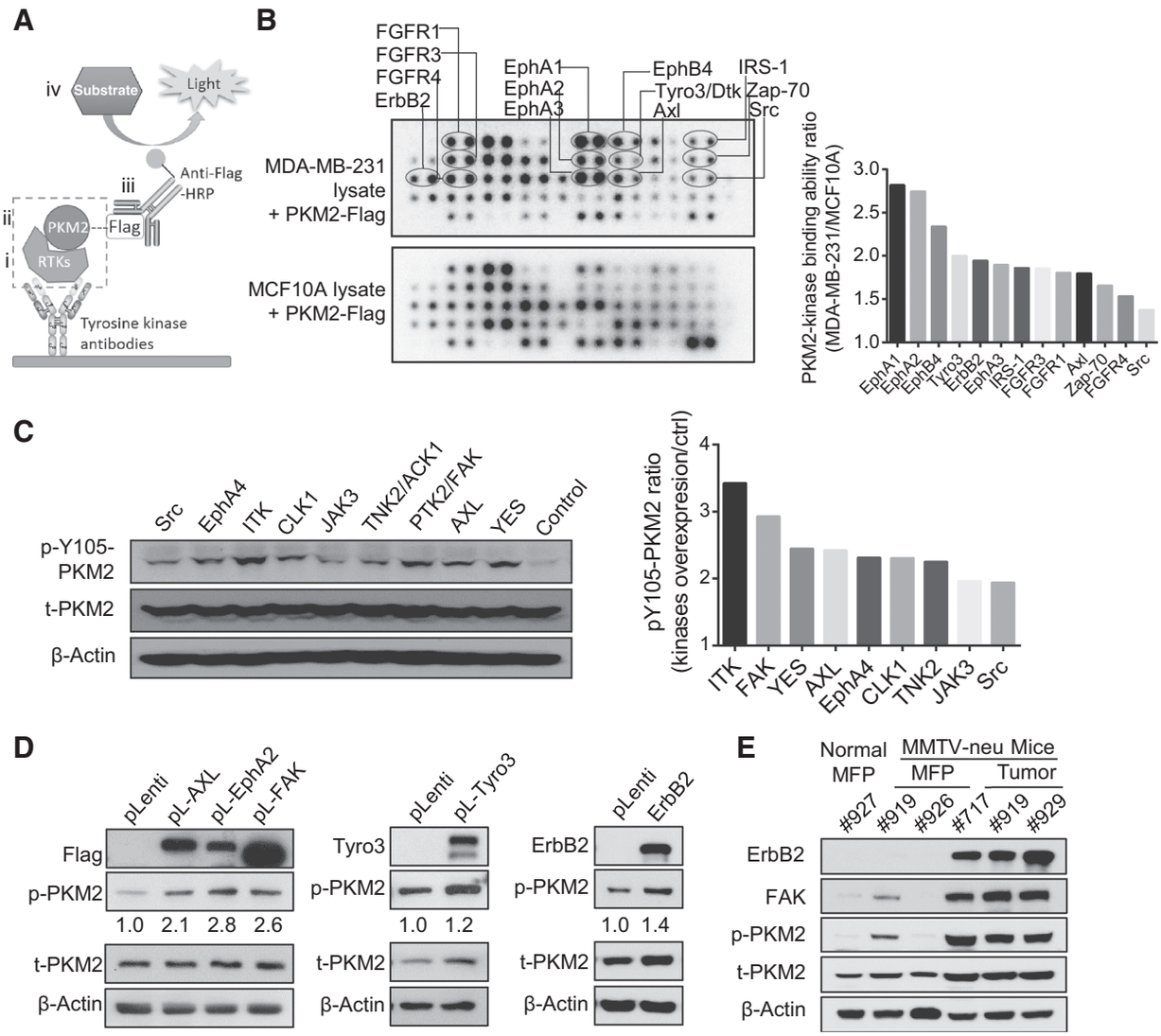

Figure 2.

Multiple oncogenic kinases phosphorylate PKM2 at Y105 in human breast cancer cells. **A,** The schematics of the modified protocol using the kinase antibody array. **i,** Kinases in the added cell lysates can be captured by corresponding antibodies in the kinase antibody array; **ii,** if a captured kinase can phosphorylate PKM2, it can bind to the purified PKM2-Flag proteins added to the array; **iii,** this interaction can be detected by anti–Flag-HRP antibodies; and **iv,** the array is developed using chemiluminescence imaging. RTK, receptor tyrosine kinase. **B,** Left, screening of PKM2-interacting kinases in MDA-MB-231 versus MCF10A cells was performed using kinase antibody array following the previously described procedures. Right, quantification of PKM2-kinase binding intensity in MDA-MB-231 versus MCF10A cells (ratio) using the ImageJ software. **C,** Left, Western blot analysis of pY105-PKM2 and total PKM2 levels in 293T cells transfected with indicated kinase expression vectors from the kinase library. Right, quantification of pY105-PKM2 in kinase-transduced cells versus vector control cells after normalizing to β-actin with ImageJ software. **D,** Western blot analysis of various kinases, pY105-PKM2, and total PKM2 levels in MCF10A cells transfected with various kinase expression vectors versus pLenti vector. ImageJ software quantification of pY105-PKM2 signals in cells transduced with kinase vectors versus pLenti vector after normalizing to β-actin. **E,** Western blot analysis of ErbB2, FAK, pY105-PKM2, and total PKM2 levels in the MFPs (from both normal mice and MMTV-neu mice) and in the mammary tumors from MMTV-neu mice.

Statistical analysis

All quantitative experiments were performed at least three independent biological repeats, and the results are presented as the mean ± SD. A one-way ANOVA (multiple groups) or *t* test (two groups) was used to compare the mean of two or more samples using the GraphPad Prism 6 software packages. $P < 0.05$ (two sided) was considered statistically significant. *, $P < 0.05$; **, $P < 0.01$; ***, $P < 0.001$, and ****, $P < 0.0001$; n.s., not statistically significant.

Results

PKM2 is essential for proliferation/transformation and is highly phosphorylated at Y105 in human breast cancer cells

To explore whether PKM2 promotes or suppresses breast cancer progression, we analyzed the survival data of 3,951 patients with breast cancer whose tumors had a high or low expression of PKM2 by the Kaplan–Meier plotter (26). The results showed that patients with PKM2 high-expression tumors had poor clinical

Published OnlineFirst February 12, 2018; DOI: 10.1158/0008-5472.CAN-17-2726

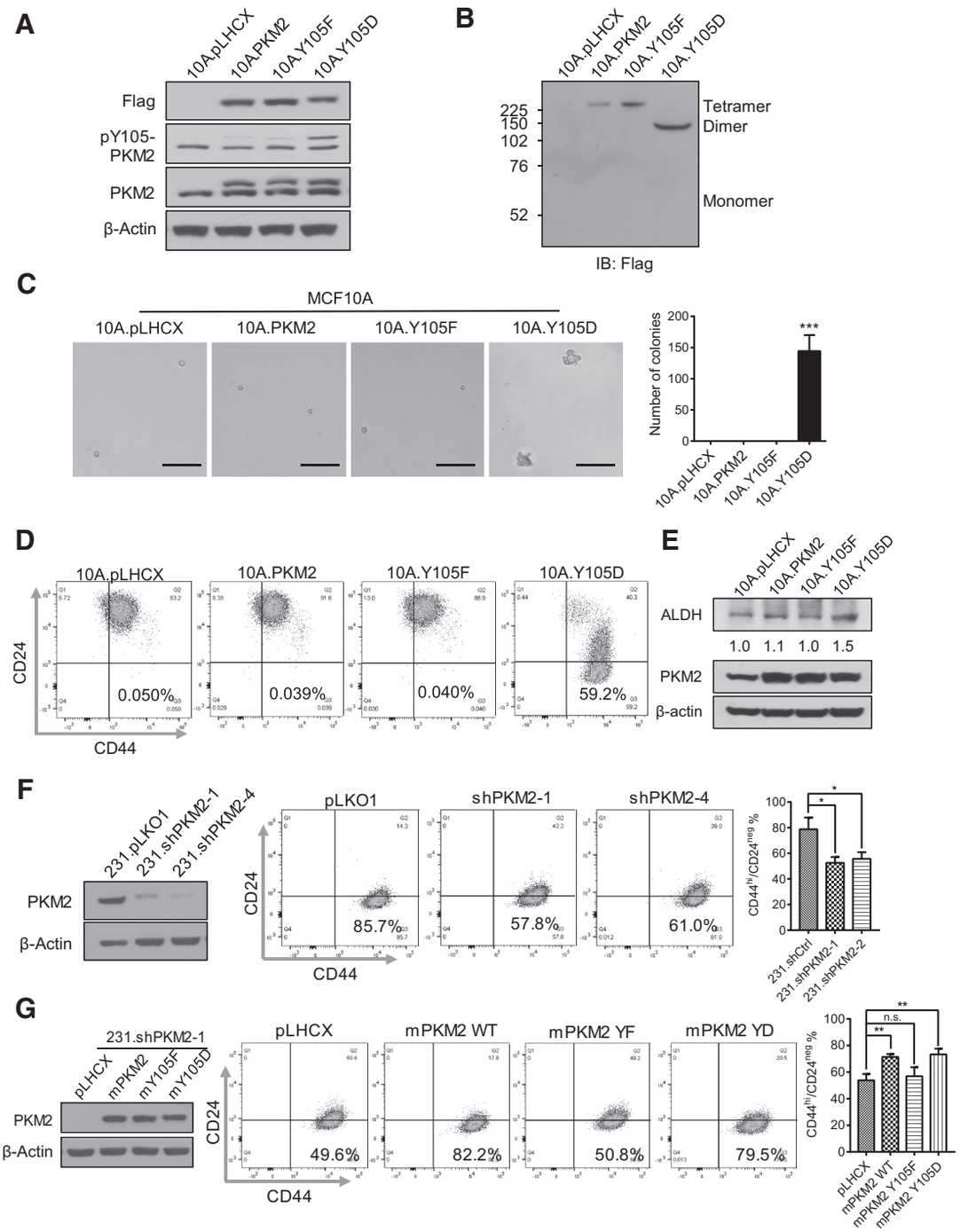

Figure 3.

Phosphorylation of PKM2-Y105 promotes transformation and induces cancer stem–like cell properties. **A,** Western blot analysis of PKM2 variants expression (with Flag tag), pY105-PKM2, and total PKM2 levels in the 10A.pLHCX, 10A.PKM2, 10A.Y105F, and 10A.Y105D cells. **B,** Western blot analysis using anti-Flag antibodies to detect PKM2 protein tetramers and dimers in the 10A.pLHCX, 10A.PKM2, 10A.Y105F, and 10A.Y105D cell lysates. **C,** Left, representative images of colony formation from the indicated MCF10A stable sublines in soft agar. Right, quantification of colonies of the indicated MCF10A stable sublines in soft agar. ***, $P < 0.001$. **D,** Flow cytometry analysis of the cancer stem–like cell population ($CD44^{hi}/CD24^{neg}$) in the 10A.pLHCX, 10A.PKM2, 10A.Y105F, and 10A.Y105D sublines. **E,** Western blot analysis of ALDH and PKM2 levels in the 10A.pLHCX, 10A.PKM2, 10A.Y105F, and 10A.Y105D cells. ImageJ software was used for quantification of ALDH normalized to β-actin. **F,** Left, Western blot analysis of PKM2 expression in MDA-MB-231 cells transfected with shCtrl, shPKM2-1, and shPKM2-2. Right, flow cytometry analysis and statistics of the cancer stem–like cell population ($CD44^{hi}/CD24^{neg}$) in the 231.shCtrl, 231.shPKM2-1, and 231.shPKM2-4 cells. *, $P < 0.05$. **G,** To avoid shRNA-mediated depletion of exogenous human PKM2, mouse PKM2 WT, PKM2-Y105F, and PKM2-Y105D were introduced into PKM2 knockdown MDA.MB.231 cells. Left, Western blot analysis of mPKM2 variants expression in 231.shPKM2-1. Right, flow cytometry analysis and statistics of the cancer stem–like cell population ($CD44^{hi}/CD24^{neg}$) in the corresponding cells. **, $P < 0.01$; n.s., not statistically significant.

Published OnlineFirst February 12, 2018; DOI: 10.1158/0008-5472.CAN-17-2726

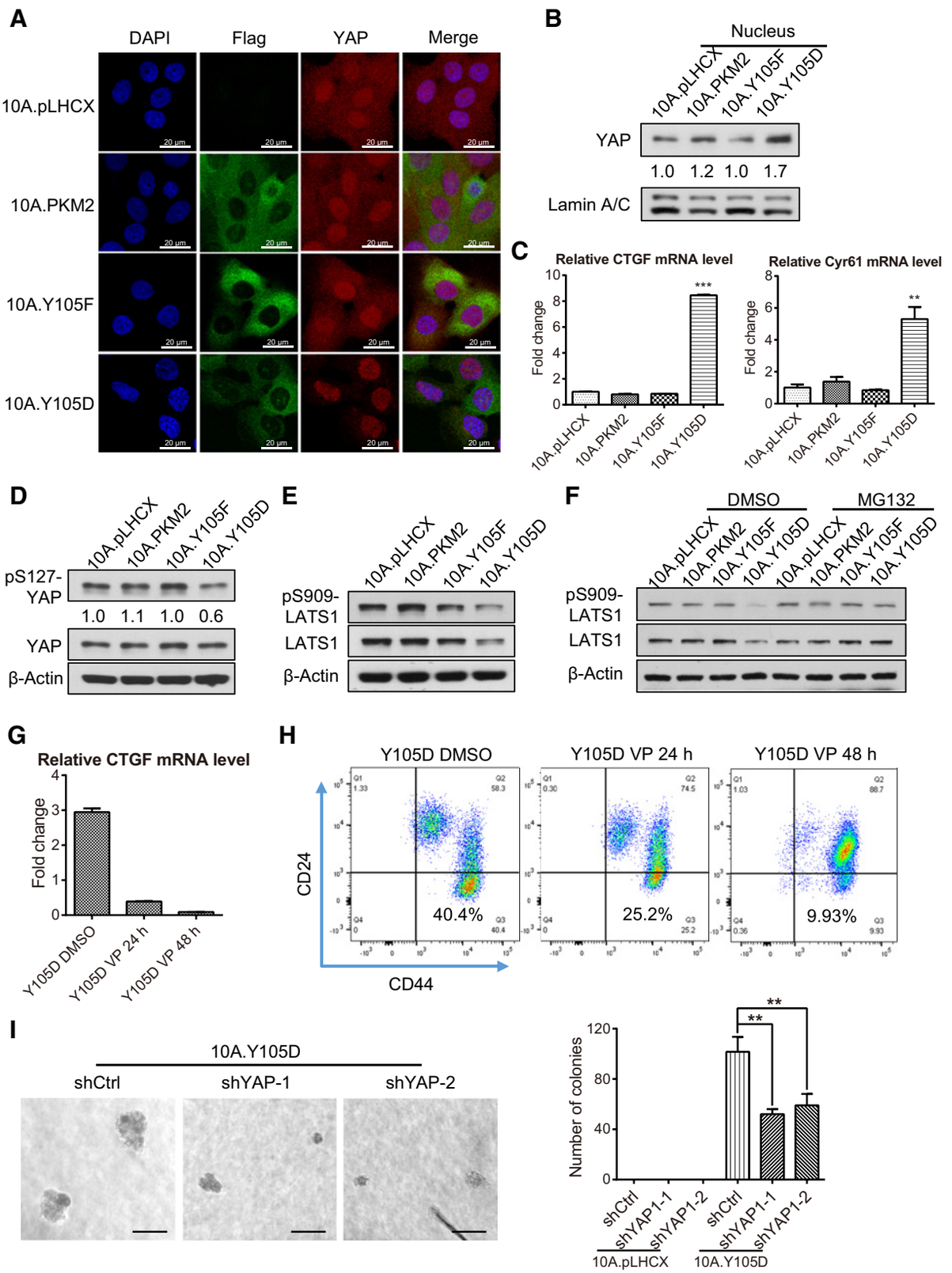

Published OnlineFirst February 12, 2018; DOI: 10.1158/0008-5472.CAN-17-2726

outcomes (median survival duration, 171.43 months vs. 216.66 months; P value < $2.8e^{-5}$; Fig. 1A), indicating that PKM2 is a risk factor for the poor prognosis of breast cancer.

Next, we examined whether PKM2 is important for cancer cell growth. Specifically knocking down PKM2 with shRNAs without the change of PKM1 (Supplementary Fig. S1A) in MDA-MB-231 (231.shPKM2) and MDA-MB-435 triple-negative breast cancer cells significantly inhibited cell proliferation (Fig. 1B; Supplementary Fig. S1B). However, PKM2 knockdown had no discernable effect on cell growth of MCF10A and MCF12A nontransformed mammary epithelial cells (Fig. 1C; Supplementary Fig. S1C). In addition, knocking down PKM2 also significantly reduced the colony formation ability of MDA-MB-231 cells in soft agar (Fig. 1D), which is a key characteristic of transformed cells. These data suggested that PKM2 is critical for breast cancer cell proliferation and transformation, whereas PKM2 has no discernible effect on nontransformed cell proliferation.

PKM2 can be allosterically activated by the upstream glycolytic metabolite FBP, which was found to promote the association of PKM2 proteins into homotetramers (3). When PKM2 tetramers dissociate into dimers, the PK activity of PKM2 decreases, which is associated with increased tumorigenicity (1). Interestingly, we found that most PKM2 proteins formed homotetramers in nontransformed mammary epithelial cells (MCF10A and MCF12A), whereas a majority of PKM2 formed dimers in cancer cells (MDA-MB-231 and MDA-MB-435; Fig. 1E).

It is known that phosphorylation of PKM2 at Y105 leads to tetramer dissociation into dimers by releasing FBP from tetramers (17). Therefore, we compared the phosphorylation of PKM2 at Y105 in various nontransformed mammary epithelial cells (MCF10A and MCF12A) versus breast cancer cells, including luminal type (MCF7, HCC1954, MDA-MB-361, and BT474) and basal type (MDA-MB-231 and Hs578T). We found that PKM2 is highly phosphorylated at Y105 in breast cancer cells versus nontransformed cells, although they have similar levels of total PKM2 expressions (Fig. 1F). Importantly, the phosphorylation level of PKM2-Y105 was higher in human invasive breast cancers than in epithelial cells, which compose a thin layer around the gland tubes of normal breast tissues, despite the similar total PKM2 protein levels (Fig. 1G). Taken together, these data suggest that PKM2 has distinct functions. In breast cancer cells, PKM2 proteins are phosphorylated at Y105 and form dimers, which are essential for cell growth and transformation; however, in nontransformed cells, most PKM2 proteins remain unphosphorylated at Y105 and form tetramers, which are dispensable for cell growth.

Multiple oncogenic kinases phosphorylate PKM2 at Y105 in human breast cancer cells

Because cancer cells accumulate significantly more phosphorylated PKM2-Y105 (pY105-PKM2), we postulated that aberrantly activated oncogenic kinases in cancer cells can induce pY105-PKM2. Activation of oncogenic tyrosine kinases is common in human breast cancers, but not in normal mammary tissues (27). To identify tyrosine kinases that may bind to PKM2 and induce PKM2 phosphorylation at Y105 in cancer cells, we used an antibody array detecting 27 receptor tyrosine kinases and 11 important kinase signaling nodes (Supplementary Table S1) for kinase screening with a modified procedure (Fig. 2A). By comparing the differences of kinase–PKM2 binding intensity between MDA-MB-231 and MCF10A cells, we identified multiple kinases with stronger binding capacity to PKM2 in MDA-MB-231 cells, including ErbB2, IRS-1, Zap-70, Src, the EphR family kinases (EphA1, EphA2, EphA3, and EphB4), the TAM family kinases (Tyro3 and AXL), and the FGFR family kinases (FGFR1, FGFR3, and FGFR4; Fig. 2B). In parallel, we performed a complementary mini-screen by selecting 33 tyrosine kinases (Supplementary Table S1) from a kinase library (18) and transfecting them into 293T cells to identify additional tyrosine kinases that induce pY105-PKM2. Among these, nine tyrosine kinases (ITK, PTK2/FAK, YES, AXL, CLK1, EphA4, TNK2/ACK1, JAK3, and Src) induced phosphorylation of PKM2 at Y105 (Fig. 2C).

Among the candidates from the above two screenings, we chose several kinases well-known to be frequently dysregulated in various cancer types (Supplementary Table S2; refs. 28, 29) and commonly activated in human breast cancers (27, 30, 31). Overexpression of AXL, EphA2, FAK, Tyro3, and ErbB2 in MCF10A cells significantly increased phosphorylation of PKM2 at Y105 (Fig. 2D). In addition, the mammary tumors of the MMTV-neu genetically engineered mice (24) had highly activated ErbB2 and FAK kinases and exhibited significantly higher pY105-PKM2 along with a moderate increase of total PKM2 proteins (Fig. 2E; Supplementary Fig. S2). These data indicated that multiple oncogenic tyrosine kinases that are frequently activated in breast cancers can phosphorylate PKM2 at Y105.

Phosphorylation of PKM2-Y105 promotes transformation and induces cancer stem–like cell properties

Because pY105-PKM2 was shown to correlate with tumor progression (17) and this phosphorylation can be induced by many oncogenic kinases, we postulated that pY105-PKM2 played a role in cell transformation. To test this, we transfected MCF10A cells with pLHCX vector control (10A.pLHCX),

Figure 4.

Phosphorylation of PKM2-Y105 induced cancer stem–like cell properties by activating YAP downstream signaling. **A,** Immunofluorescence imaging of the expression and localization of exogenous PKM2 variants (indicated by Flag antibody, green), YAP (red), and the nucleus (DAPI, blue) in the 10A.pLHCX, 10A.PKM2, 10A.Y105F, and 10A.Y105D cells. **B,** Western blot analysis of YAP protein levels in the nuclear fraction of the 10A.pLHCX, 10A.PKM2, 10A.Y105F, and 10A.Y105D cells. ImageJ software was used for quantification of YAP band intensity that was normalized to Lamin A/C. **C,** The CTGF and Cyr61 mRNA levels in the 10A.pLHCX, 10A.PKM2, 10A.Y105F, and 10A.Y105D cells were measured by quantitative PCR. **, $P < 0.01$; ***, $P < 0.001$. **D,** Western blot analysis of pS127-YAP and total YAP protein levels in the 10A.pLHCX, 10A.PKM2, 10A.Y105F, and 10A.Y105D sublines. ImageJ software was used for quantification of each subline's pS127-YAP level (normalized to β-actin) compared with that in the 10A.pLHCX vector control cells. **E,** Western blot analysis of the pS909-LATS1 and total LATS1 levels in the 10A.pLHCX, 10A.PKM2, 10A.Y105F, and 10A.Y105D sublines. **F,** Western blot analysis of the pS909-LATS1 and total LATS1 levels in the MCF10A sublines treated with DMSO or 10 μmol/L MG132 for 4 hours. **G,** The CTGF mRNA level in 10A.Y105D cells treated with DMSO (as control, first bar) and 10 μmol/L VP for 24 hours or 48 hours. **H,** Flow cytometry analysis of the cancer stem–like cell population ($CD44^{hi}/CD24^{neg}$) in 10A.Y105D cells treated as in **G**. **I,** Representative images (left) and quantification (right) of the soft-agar colonies from 10A.Y105D cells transfected with control shRNA (shCtrl) or two different YAP shRNAs (shYAP-1 and shYAP-2). **, $P < 0.01$.

Published OnlineFirst February 12, 2018; DOI: 10.1158/0008-5472.CAN-17-2726

Flag-tagged WT human PKM2 (10A.PKM2), a phospho-defective mutant (10A.Y105F), and a phosphomimetic mutant (10A.Y105D; Fig. 3A). Remarkably, the phosphomimetic PKM2-Y105D proteins formed dimers that were predominant in cancer cells, whereas PKM2 WT and PKM2-Y105F proteins formed tetramers, similar to the PKM2 conformation in non-transformed cells (Fig. 3B).

To determine whether phosphorylation of PKM2-Y105 is sufficient to promote cell transformation, we examined whether these cells can acquire anchorage-independent growth ability in soft agar (32). Strikingly, only 10A.Y105D cells formed colonies in soft agar; none of the other three MCF10A sublines grew into colonies (Fig. 3C). This finding indicates that phosphorylation of PKM2 at Y105 induces cell transformation. Previous studies showed that cell transformation was associated with increased glycolysis (23), and the glycolytic function of PKM2 promotes tumor growth (17). Consistently, 10A.Y105D cells showed an increased glycolysis (Supplementary Table S3) compared with the other three MCF10A sublines.

Importantly, anchorage-independent growth is an essential characteristic of cancer stem–like cells, which can be identified by the $CD44^{hi}/CD24^{neg}$ marker in human breast cancer (33). Indeed, expression of PKM2-Y105D in MCF10A cells induced a high percentage (>59%) of cancer stem–like cell population, whereas expression of pLHCX vector, PKM2 WT, and PKM2-Y105F did not (Fig. 3D). The 10A.Y105D cells also showed an increased expression of ALDH (Fig. 3E), a stemness biomarker of human mammary stem cells (34). On the other hand, knocking down PKM2 in MDA-MB-231 (231.shPKM2) breast cancer cells that have high phosphorylation at Y105 of PKM2 (Fig. 1F) led to reduced cancer stem–like cell populations (Fig. 3F). Introducing mouse WT PKM2 (98% identical to human PKM2 protein) and PKM2-Y105D, but not PKM2-Y105F, into 231.shPKM2 cells rescued their cancer stem–like cell populations (Fig. 3G). Taken together, these data suggest that phosphorylation of PKM2-Y105 promotes cell transformation and induces cancer stem–like cell properties.

Phosphorylation of PKM2-Y105 induces cancer stem–like cell properties by activating YAP downstream signaling

Increasing evidence has shown that the Hippo pathway is tied to the acquisition of breast cancer stem cell (CSC)–related traits (35). YAP and transcriptional coactivator with a PDZ-binding motif (TAZ) are the major downstream effectors of the Hippo pathway, regulating tissue progenitor cell growth and tumorigenesis (36). The PKM2 interaction network analyzed by the Genemania online tool revealed connections between PKM2 and YAP/TAZ (TAZ is also known as WWTR1; Supplementary Fig. S3A). Activation of YAP enhances multiple processes during tumor progression (37). Thus, we investigated whether YAP is involved in the pY105-PKM2–induced cancer stem–like cell properties. Although knocking down PKM2 in MCF10A cells did not alter the YAP protein or mRNA levels (Supplementary Fig. S3B and S3C), immunofluorescent staining showed that the 10A.Y105D cells had less cytoplasmic YAP proteins compared with nontransformed MCF10A sublines (Fig. 4A). Furthermore, we also detected an increase of YAP proteins in the nuclear fraction of 10A.Y105D cells compared with other MCF10A sublines (Fig. 4B), whereas the cytoplasmic YAP proteins were reduced in the 10A.Y105D cells (Supplementary Fig. S3D). In addition, 231.shPKM2 cells had reduced nuclear YAP (Supplementary Fig. S3E), whereas reexpression of WT PKM2 or introducing PKM2-Y105D mutant into 231.shPKM2 cells rescued the nuclear YAP reduction (Supplementary Fig. S3F).

Nuclear YAP functions as a transcriptional cofactor to initiate transcription by interacting with TEA domain transcription factors 1–4 (TEAD1–4; ref. 37). The 10A.Y105D cells with increased nuclear YAP proteins exhibited significantly higher transcription level of YAP downstream targets, such as CTGF and CYR61 (Fig. 4C). In addition, there is a strong correlation between PKM2 and YAP downstream effector CTGF in the Esserman breast cancer dataset (Supplementary Fig. S4A). These results indicate that pY105-PKM2 activates YAP downstream signaling by increasing YAP nuclear translocation.

It is known that YAP can be retained in the cytoplasm by 14-3-3 when YAP is phosphorylated at serine 127 (S127; ref. 38). Consistent with the reduction of cytoplasmic YAP in the 10A.Y105D cells (Fig. 4A; Supplementary Fig. S3D), pS127-YAP decreased in the 10A.Y105D cells compared with that in other MCF10A sublines (Fig. 4D), but the total YAP protein or mRNA levels were similar among all four sublines (Fig. 4D; Supplementary Fig. S4B).

YAP-S127 is specifically phosphorylated by the Hippo kinase LATS1 (39). Interestingly, the 10A.Y105D cells exhibited a reduction in pS909-LATS1 (kinase activation marker of LATS1) and total LATS1 protein (Fig. 4E), but no decrease of LATS1 mRNA level (Supplementary Fig. S4C). Thus, we tested whether the decrease of LATS1 protein in the 10A.Y105D cells was due to reduced protein stability. Indeed, after treatment with the protease inhibitor MG132, both the LATS1 protein and pS909-LATS1 were rescued in the 10A.Y105D cells to a similar level as in other MCF10A sublines (Fig. 4F). These data indicate that the reduction of LATS1 protein level in the 10A.Y105D cells is due to protein destabilization.

To determine whether YAP contributed to the cancer stem–like cell population induced by pY105-PKM2, we evaluated the $CD44^{hi}/CD24^{neg}$ population when YAP function was inhibited by the YAP/TAZ inhibitor VP. VP treatment effectively inhibited YAP downstream signaling (as indicated by the CTGF and Cyr61 mRNA level; Fig. 4G) and decreased the $CD44^{hi}/CD24^{neg}$ population in the 10A.Y105D cells (Fig. 4H). Knocking down YAP with siRNAs also resulted in a moderate decrease of the $CD44^{hi}/CD24^{neg}$ population in the 10A.Y105D cells (Supplementary Fig. S4D); this decrease could partly be due to the compensational increase of TAZ (Supplementary Fig. S4E), as previously reported (40). Importantly, knocking down YAP with shRNAs significantly impaired the anchorage-independent growth ability of the 10A.Y105D cells (Fig. 4I) and had a more profound effect on the proliferation of the 10A.Y105D cells than that of 10A.pLHCX cells (Supplementary Fig. S4F), suggesting that YAP plays an important role in the pY105-PKM2–induced transformation and cancer stem–like cell properties.

Abrogation of YAP downstream signaling inhibits oncogenic kinase–induced cancer stem–like cell population

Given that multiple kinases phosphorylate PKM2 at Y105 (Fig. 2B–D), we tested whether they can induce cancer stem–like cell properties. Indeed, overexpression of ErbB2, AXL, EPHA2, FAK, and Tyro3 increased the $CD44^{hi}/CD24^{neg}$ cancer stem–like cell population in MCF10A cells (Fig. 5A). Among these candidate kinases, ErbB2 was the strongest inducer. Inhibition of YAP/TAZ

Published OnlineFirst February 12, 2018; DOI: 10.1158/0008-5472.CAN-17-2726

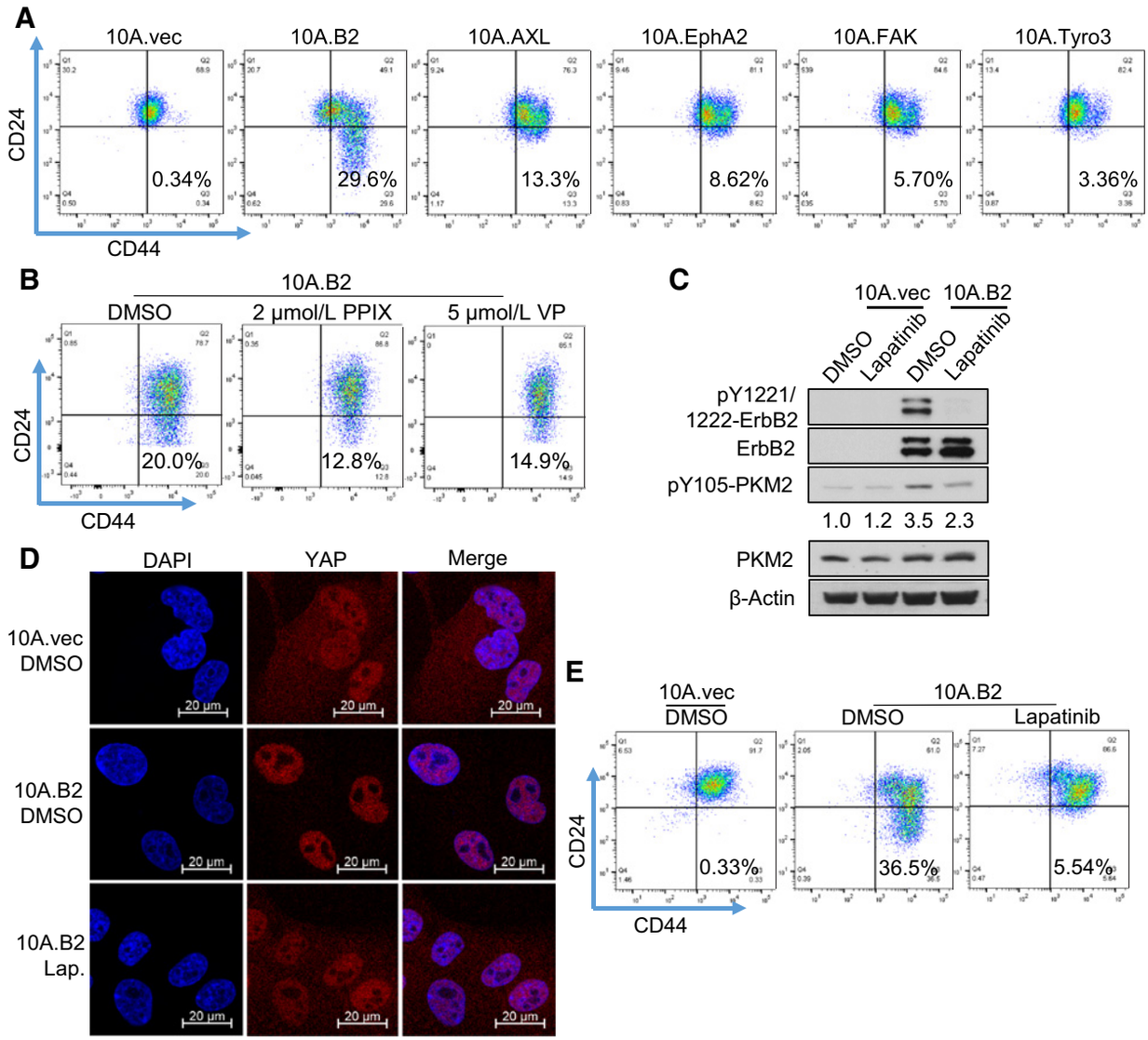

Figure 5.

Abrogation of YAP downstream signaling inhibited oncogenic kinase–induced cancer stem–like cell population *in vitro*. **A,** Flow cytometry analysis of the cancer stem–like cell populations ($CD44^{hi}/CD24^{neg}$) in MCF10A cells transfected with expression vectors of indicated kinases that can phosphorylate PKM2-Y105. **B,** Flow cytometry analysis of the cancer stem–like cell population ($CD44^{hi}/CD24^{neg}$) in the 10A.B2 cells treated with DMSO (as controls), 2 μmol/L PPIX, or 5 μmol/L VP. **C,** Western blot analysis of the pY1221/1222-ErbB2, total ErbB2 protein, pY105-PKM2, and total PKM2 protein levels in the 10A.vec and 10A.B2 cells after treatment with DMSO or lapatinib (1 μmol/L) for 24 hours. Quantification of pY105-PKM2 comparing different samples with 10A.vec. DMSO (normalized by β-actin) was conducted by Image J software. **D,** Representative immunofluorescent staining showing the colocalization of YAP protein (red) and nuclear (DAPI, blue) in the DMSO-treated 10A.vec cells and the DMSO- or lapatinib-treated (1 μmol/L) 10A.B2 cells. **E,** Flow cytometry analysis of the cancer stem–like cell population ($CD44^{hi}/CD24^{neg}$) in the DMSO-treated 10A.vec cells and the DMSO- or lapatinib-treated (1 μmol/L) 10A.B2 cells.

using the chemical inhibitors PPIX and VP (41) effectively reduced the $CD44^{hi}/CD24^{neg}$ population in ErbB2-transfected MCF10A cells (10A.B2; Fig. 5B; ref. 20), suggesting that the ErbB2-induced cancer stem–like cell population was mediated by YAP activation.

Next, we tested if blocking ErbB2 kinase activity with the EGFR/ErbB2 kinase inhibitor lapatinib can inhibit YAP activation and reduce cancer stem–like cell population. Lapatinib treatment effectively inhibited ErbB2 phosphorylation and decreased pY105-PKM2 induced by ErbB2 expression (Fig. 5C). Furthermore, the increased nuclear translocation of YAP in 10A.B2 cells was inhibited by lapatinib, leading to cytoplasmic retention of YAP proteins (Fig. 5D). Importantly, lapatinib treatment dramatically reduced cancer stem–like cell population in 10A.B2 cells (Fig. 5E).

Compared with the mammary epithelial cells in WT FVB mice, ErbB2 high-expressing mammary tumors in $PTEN^{-/-}$/NIC mice (24) exhibited significantly increased ErbB2 phosphorylation ($P < 0.0001$), total ErbB2 proteins ($P < 0.0005$), PKM2-Y105 phosphorylation ($P < 0.005$), and nuclear YAP proteins ($P < 0.005$). Remarkably, lapatinib treatment highly significantly

Published OnlineFirst February 12, 2018; DOI: 10.1158/0008-5472.CAN-17-2726

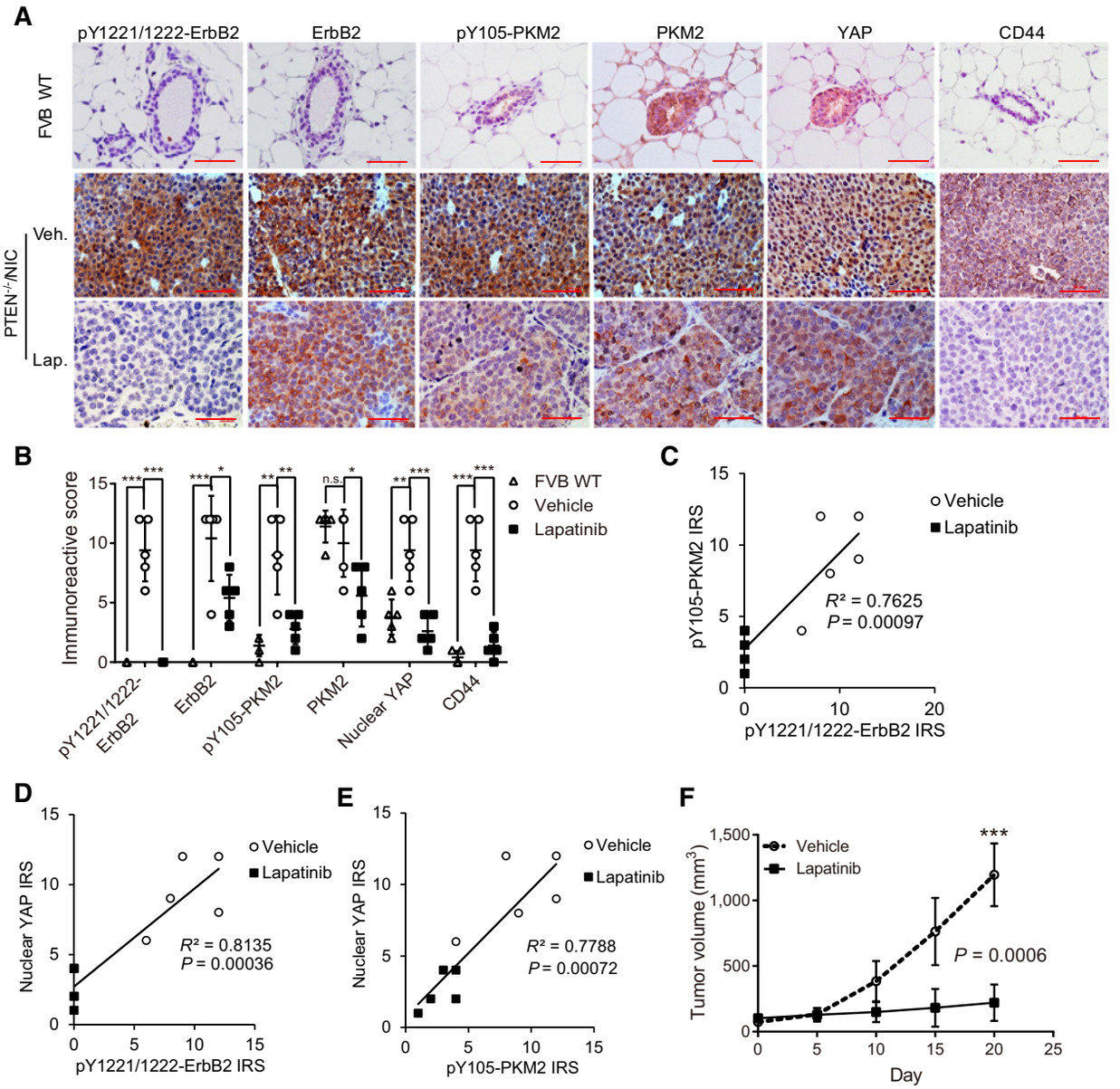

Figure 6.

ErbB2 kinase inhibitor suppressed pY105-PKM2, YAP nuclear translocation, cancer stem–like cell properties, and mammary tumor growth *in vivo*. **A,** Representative IHC staining images of expression and localization of pY1221/1222-ErbB2, total ErbB2, pY105-PKM2, total PKM2, YAP proteins, and CD44 in the MFP of WT mice and in mammary tumors from vehicle- or lapatinib (Lap.)-treated (100 mg/kg, daily) PTEN$^{-/-}$/NIC mice. **B,** Quantification of the pY1221/1222-ErbB2, ErbB2, pY105-PKM2, PKM2, nuclear YAP, and CD44 IRS in the MFP of WT mice and mammary tumors from vehicle- or lapatinib-treated PTEN$^{-/-}$/NIC mice. *, $P < 0.05$; **, $P < 0.01$; ***, $P < 0.001$; n.s., not statistically significant. **C,** Correlation between the pY1221/1222-ErbB2 and the pY105-PKM2 IRS in the vehicle- or lapatinib-treated mammary tumors from PTEN$^{-/-}$/NIC mice. **D,** Correlation between the pY1221/1222-ErbB2 and the nuclear YAP IRS in the vehicle- or lapatinib-treated mammary tumors from PTEN$^{-/-}$/NIC mice. **E,** Correlation between the pY105-PKM2 and the nuclear YAP IRS in the vehicle- or lapatinib-treated mammary tumors from PTEN$^{-/-}$/NIC mice. **F,** Growth curves of the vehicle- versus lapatinib-treated mammary tumors from PTEN$^{-/-}$/NIC mice ($n = 5$ for each group).

decreased ErbB2 phosphorylation ($P < 0.0001$), PKM2-Y105 phosphorylation ($P < 0.005$), and nuclear YAP proteins ($P < 0.001$) in mammary tumors, with moderate reductions of total ErbB2 and PKM2 (Fig. 6A and B). Notably, ErbB2 phosphorylation significantly correlated with pY105-PKM2 and YAP nuclear localization (Fig. 6C and D; Supplementary Fig. S5A and S5B), and there was also a strong correlation between pY105-PKM2 and YAP nuclear localization (Fig. 6E; Supplementary Fig. S5C). Importantly, ErbB2-induced pY105-PKM2 was strongly correlated with cancer stem–like cell marker CD44 expression (Supplementary Fig. S5D). Lapatinib treatment, which reduced PKM2-Y105 phosphorylation, significantly decreased

Published OnlineFirst February 12, 2018; DOI: 10.1158/0008-5472.CAN-17-2726

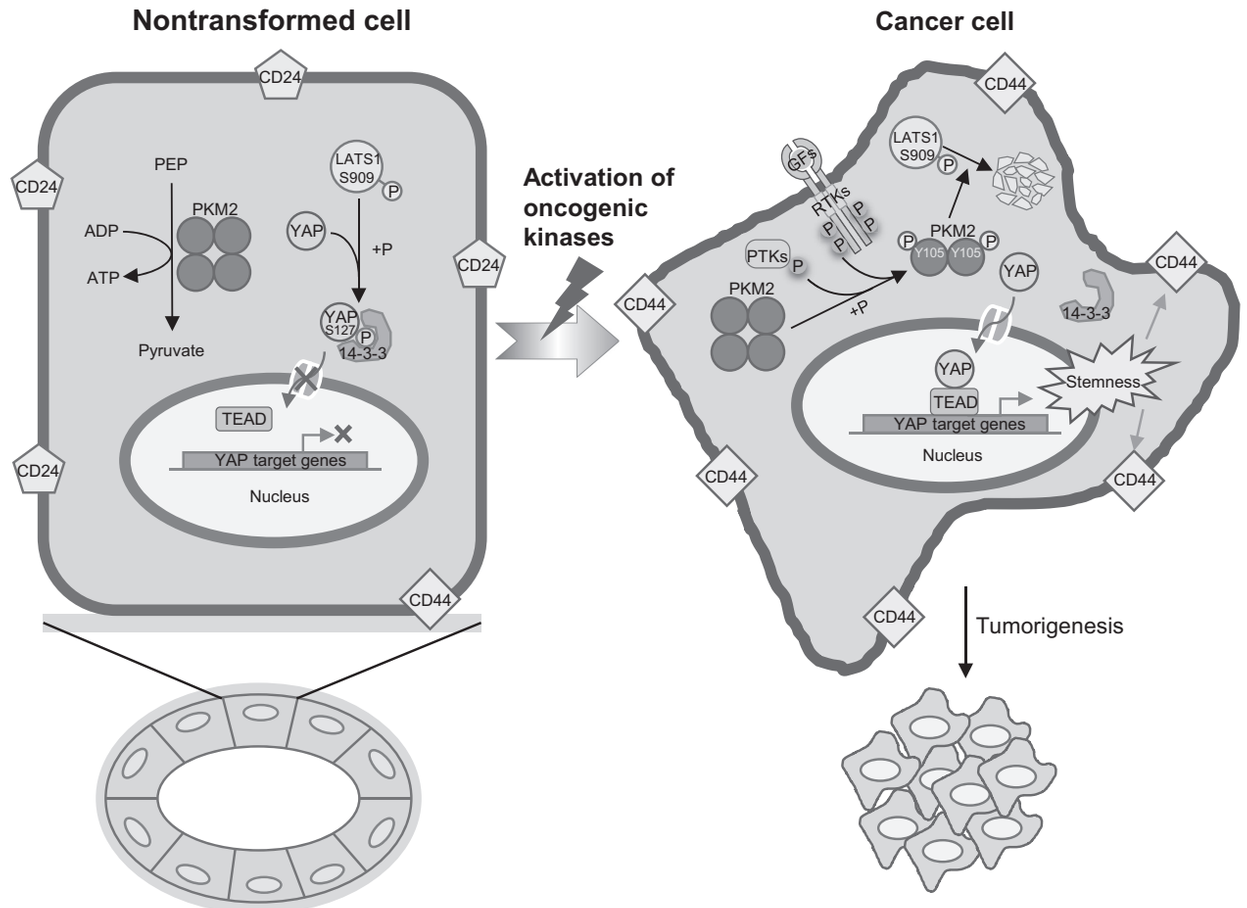

Figure 7.

A model of the dichotomous functions of PKM2 in nontransformed cells versus cancer cells. Left, in nontransformed epithelial cells, PKM2 proteins remain mostly unphosphorylated and form tetramers, which can efficiently catalyze pyruvate and ATP production. Activated Hippo kinase LATS1 (indicated by pS909) can phosphorylate YAP at S127, which can be recognized and bound by the 14-3-3 protein, leading to cytoplasmic retention of YAP proteins. Right, during cell transformation, multiple receptor tyrosine kinases (RTK) and protein tyrosine kinases (PTK) are activated, which can phosphorylate PKM2 at Y105. Phosphorylated PKM2 proteins dissociate into dimers and promote LATS1 degradation. Without LATS1-mediated phosphorylation, YAP translocates into the nucleus and cooperates with TEAD to activate target genes transcription, further inducing $CD44^{hi}/CD24^{neg}$ cancer stem–like population to promote tumorigenesis.

CD44 expression ($P < 0.005$; Fig. 6A and B). Furthermore, lapatinib treatment led to a significant suppression of mammary tumor growth in $PTEN^{-/-}$/NIC mice (Fig. 6F). Taken together, activation of oncogenic kinases, such as ErbB2, can induce phosphorylation of PKM2-Y105. Phospho-Y105-PKM2 leads to YAP nuclear translocation and enhances the $CD44^{hi}/CD24^{neg}$ cancer stem–like cell population, which partly contributes to tumor progression (Fig. 7, right).

Discussion

Together, PKM2 has dichotomous functions in nontransformed cells (nononcogenic) versus in cancer cells (tumorigenic). We found that in nontransformed mammary epithelial cells, unphosphorylated PKM2 proteins form tetramers with high PK activity (Fig. 7, left). The unphosphorylated PKM2 is dispensable for cell growth and transformation because PKM1 predominantly functions in maintaining the homeostasis of glucose metabolism in normal tissue when PKM2 is absent (12). However, in transformed tumor cells, PKM2 proteins are phosphorylated at Y105 by various oncogenic kinases and dissociate into dimers. The pY105-PKM2 promotes YAP nuclear translocation and increases cancer stem–like cells, becoming essential for tumor cell growth and transformation (Fig. 7, right). The functions of PKM2 could be altered by the different status of PKM2-Y105 phosphorylation, which is dictated by the activities of oncogenic kinases (Fig. 7).

The above findings can clarify some seemingly conflicting reports on the role of PKM2 in tumor progression. For example, PKM2 knockout inhibited leukemia initiation in mice injected with the BCR-ABL–transduced bone marrow cells, suggesting that PKM2 is a tumor promoter (42). Because BCR-ABL kinase was also found to phosphorylate PKM2-Y105 (17), our explanation is that the BCR-ABL–mediated PKM2-Y105 phosphorylation promoted leukemia initiation in this case. On the other hand, depletion of PKM2 in a *Brca1*-loss–driven mammary tumor model did not delay tumor onset. The reason is that without activation of

Published OnlineFirst February 12, 2018; DOI: 10.1158/0008-5472.CAN-17-2726

oncogenic kinases, PKM2 cannot contribute to tumorigenesis in *Brca1*-loss mammary epithelial cells. Therefore, part of the PKM2 oncogenic function is driven by its upstream oncogenic kinase activities.

In addition to metabolic functions of PKM2 in promoting tumor growth (7, 17), we revealed a novel mechanism that pY105-PKM2 induced cancer stem–like cell properties by promoting YAP nuclear translocation. Activation of YAP was shown to be critical for cell transformation (43) and correlated with cancer stem–like cell properties (35). Specifically, we found that pY105-PKM2 led to the destabilization of the Hippo kinase LATS1, thus reducing phosphorylation of YAP at S127 and preventing YAP cytoplasmic retention by 14-3-3 proteins (44). Consequently, S127-unphosphorylated YAP proteins translocated into the nucleus and activated downstream targets to promote malignant transformation. It will be fascinating to explore how PKM2 cross-talks to the Hippo pathway and regulates LATS1 protein stability in future studies.

CSCs, or cancer-initiating cells, are defined as a subset of self-renewal cancer cells. Although the function of CSCs in tumorigenicity needs further characterization (45), substantial studies indicate that an important feature of CSCs is their tumor initiation capability, frequently indicated or measured by tumor formation in xenograft models (46, 47). The CSCs in human breast cancers were first marked as $CD44^{+}/CD24^{-/low}$, and 1,000 of $CD44^{+}/CD24^{-/low}$ CSCs, but not $CD44^{+}/CD24^{high}$ breast cancer cells, could induce tumors that can be serially transplanted in NOD/SCID mice (33). Another marker of CSCs in breast cancer is ALDH, and 500 of $ALDH^{+}$ CSCs, but not $ALDH^{-}$ breast cancer cells, also formed xenograft tumors (34). In this study, we found that pY105-PKM2 significantly enhanced $CD44^{hi}/CD24^{neg}$ and/or $ALDH^{+}$ cancer stem–like cells in MCF10A and MDA.MB.231 cell lines (Fig. 3D–G). These cancer stem–like cells also demonstrated self-renewal capacity in soft-agar colony formation assays (Figs. 1D and 3C; refs. 48, 49). Importantly, compared with PKM2-Y105F–transduced H1299 lung cancer cells, PKM2 WT-transduced H1299 cells, in which PKM2-Y105 could be phosphorylated by activated oncogenic kinases and hence have more CSCs, induced significantly bigger xenograft tumors (17). These previous studies and our new findings support the notion that pY105-PKM2–induced cancer stem–like cells contribute, at least partly, to breast cancer tumorigenicity.

The intervention of cancer metabolic dysregulations has been considered as a promising strategy for cancer therapy. However, direct modulation of PKM2 may break the balance of metabolism (50); therefore, targeting oncogenic activation of PKM2 could be an alternative effective strategy. Our kinase screening identified multiple tyrosine kinases that phosphorylate PKM2 at Y105, providing multiple targets for reversing the PKM2 oncogenic functions. As a proof-of-concept study, inhibiting one of the PKM2 upstream kinases ErbB2 with lapatinib significantly reduced pY105-PKM2 and nuclear YAP, decreased cancer stem–like cell population, and inhibited tumor growth in ErbB2/neu-overexpressing mammary tumors (Fig. 6). Therefore, identifying and targeting these PKM2 upstream regulators with various kinase inhibitors can be a therapeutic strategy to inhibit PKM2 oncogenic functions in specific cancer types. As a key node of many oncogenic kinase signaling cascades, pY105-PKM2 may also serve as a biomarker for transformation and potential of tumorigenesis.

Disclosure of Potential Conflicts of Interest

No potential conflicts of interest were disclosed.

Authors' Contributions

Conception and design: Z. Zhou, M. Li, J. Chen, Z. Songyang, D. Yu
Development of methodology: Z. Zhou, M. Li, L. Zhang, H. Zhao, D. Yu
Acquisition of data (provided animals, acquired and managed patients, provided facilities, etc.): Z. Zhou, M. Li, L. Zhang, H. Zhao, Ö. Şahin, D. Yu
Analysis and interpretation of data (e.g., statistical analysis, biostatistics, computational analysis): Z. Zhou, M. Li, L. Zhang, Ö. Şahin, D. Yu
Writing, review, and/or revision of the manuscript: Z. Zhou, M. Li, L. Zhang, J.J. Zhao, Z. Songyang, D. Yu
Administrative, technical, or material support (i.e., reporting or organizing data, constructing databases): Z. Zhou, H. Zhao, D. Yu
Study supervision: D. Yu

Acknowledgments

This work was supported by the MD Anderson Cancer Center Support Grants CA016672, R01-CA184836 (D. Yu), R01-CA112567 (D. Yu), R01-CA208213 (D. Yu), and R21-CA223102 (D. Yu); China Medical University Research Fund (D. Yu); R21-CA211653 (Z. Songyang); CPRIT RP160462 (Z. Songyang); The Welch Foundation Q-1673 (Z. Songyang); and China Scholarship Council 201506380035 (Z. Zhou). D. Yu is the Hubert L. & Olive Stringer Distinguished Chair in Basic Science at MDACC.

The authors thank MDACC Functional Genomics Core and Flow Cytometry Core, Sequencing and Microarray Facility, Animal Core Facilities, Research Histology Core for technical support, Department of Scientific Publications of MDACC for article revision, and members from Dr. Dihua Yu's laboratory for insightful discussions.

The costs of publication of this article were defrayed in part by the payment of page charges. This article must therefore be hereby marked *advertisement* in accordance with 18 U.S.C. Section 1734 solely to indicate this fact.

Received September 6, 2017; revised December 27, 2017; accepted February 6, 2018; published first February 12, 2018.

References

1. Mazurek S, Boschek CB, Hugo F, Eigenbrodt E. Pyruvate kinase type M2 and its role in tumor growth and spreading. Semin Cancer Biol 2005;15:300–8.
2. Takenaka M, Yamada K, Lu T, Kang R, Tanaka T, Noguchi T. Alternative splicing of the pyruvate kinase M gene in a minigene system. Eur J Biochem 1996;235:366–71.
3. Ashizawa K, Willingham MC, Liang CM, Cheng SY. In vivo regulation of monomer-tetramer conversion of pyruvate kinase subtype M2 by glucose is mediated via fructose 1,6-bisphosphate. J Biol Chem 1991;266:16842–6.
4. Dombrauckas JD, Santarsiero BD, Mesecar AD. Structural basis for tumor pyruvate kinase M2 allosteric regulation and catalysis. Biochemistry 2005;44:9417–29.
5. Dayton TL, Jacks T, Vander Heiden MG. PKM2, cancer metabolism, and the road ahead. EMBO Rep 2016;17:1721–30.
6. Goldberg MS, Sharp PA. Pyruvate kinase M2-specific siRNA induces apoptosis and tumor regression. J Exp Med 2012;209:217–24.
7. Christofk HR, Vander Heiden MG, Harris MH, Ramanathan A, Gerszten RE, Wei R, et al. The M2 splice isoform of pyruvate kinase is important for cancer metabolism and tumour growth. Nature 2008;452:230–3.
8. Vander Heiden MG, Locasale JW, Swanson KD, Sharfi H, Heffron GJ, Amador-Noguez D, et al. Evidence for an alternative glycolytic pathway in rapidly proliferating cells. Science 2010;329:1492–9.

Published OnlineFirst February 12, 2018; DOI: 10.1158/0008-5472.CAN-17-2726

9. Yang W, Xia Y, Hawke D, Li X, Liang J, Xing D, et al. PKM2 phosphorylates histone H3 and promotes gene transcription and tumorigenesis. Cell 2012;150:685–96.
10. Yang W, Zheng Y, Xia Y, Ji H, Chen X, Guo F, et al. ERK1/2-dependent phosphorylation and nuclear translocation of PKM2 promotes the Warburg effect. Nat Cell Biol 2012;14:1295–304.
11. Liang J, Cao R, Zhang Y, Xia Y, Zheng Y, Li X, et al. PKM2 dephosphorylation by Cdc25A promotes the Warburg effect and tumorigenesis. Nat Commun 2016;7:12431.
12. Israelsen WJ, Dayton TL, Davidson SM, Fiske BP, Hosios AM, Bellinger G, et al. PKM2 isoform-specific deletion reveals a differential requirement for pyruvate kinase in tumor cells. Cell 2013;155:397–409.
13. Dayton TL, Gocheva V, Miller KM, Israelsen WJ, Bhutkar A, Clish CB, et al. Germline loss of PKM2 promotes metabolic distress and hepatocellular carcinoma. Genes Dev 2016;30:1020–33.
14. Schlessinger J. Cell signaling by receptor tyrosine kinases. Cell 2000; 103:211–25.
15. Blume-Jensen P, Hunter T. Oncogenic kinase signalling. Nature 2001; 411:355–65.
16. Christofk HR, Vander Heiden MG, Wu N, Asara JM, Cantley LC. Pyruvate kinase M2 is a phosphotyrosine-binding protein. Nature 2008;452:181–6.
17. Hitosugi T, Kang S, Vander Heiden MG, Chung TW, Elf S, Lythgoe K, et al. Tyrosine phosphorylation inhibits PKM2 to promote the Warburg effect and tumor growth. Sci Signal 2009;2:ra73.
18. Boehm JS, Zhao JJ, Yao J, Kim SY, Firestein R, Dunn IF, et al. Integrative genomic approaches identify IKBKE as a breast cancer oncogene. Cell 2007;129:1065–79.
19. Debnath J, Muthuswamy SK, Brugge JS. Morphogenesis and oncogenesis of MCF-10A mammary epithelial acini grown in three-dimensional basement membrane cultures. Methods 2003;30:256–68.
20. Lu J, Guo H, Treekitkarnmongkol W, Li P, Zhang J, Shi B, et al. 14-3-3zeta Cooperates with ErbB2 to promote ductal carcinoma in situ progression to invasive breast cancer by inducing epithelial-mesenchymal transition. Cancer Cell 2009;16:195–207.
21. Zhang L, Zhang S, Yao J, Lowery FJ, Zhang Q, Huang WC, et al. Microenvironment-induced PTEN loss by exosomal microRNA primes brain metastasis outgrowth. Nature 2015;527:100–4.
22. Zhang S, Huang WC, Zhang L, Zhang C, Lowery FJ, Ding Z, et al. SRC family kinases as novel therapeutic targets to treat breast cancer brain metastases. Cancer Res 2013;73:5764–74.
23. Chang CC, Zhang C, Zhang Q, Sahin O, Wang H, Xu J, et al. Upregulation of lactate dehydrogenase a by 14-3-3zeta leads to increased glycolysis critical for breast cancer initiation and progression. Oncotarget 2016;7:35270–83.
24. Sahin O, Wang Q, Brady SW, Ellis K, Wang H, Chang CC, et al. Biomarker-guided sequential targeted therapies to overcome therapy resistance in rapidly evolving highly aggressive mammary tumors. Cell Res 2014;24: 542–59.
25. Fedchenko N, Reifenrath J. Different approaches for interpretation and reporting of immunohistochemistry analysis results in the bone tissue - a review. Diagn Pathol 2014;9:221.
26. Gyorffy B, Lanczky A, Eklund AC, Denkert C, Budczies J, Li Q, et al. An online survival analysis tool to rapidly assess the effect of 22,277 genes on breast cancer prognosis using microarray data of 1,809 patients. Breast Cancer Res Treat 2010;123:725–31.
27. Wu X, Zahari MS, Ma B, Liu R, Renuse S, Sahasrabuddhe NA, et al. Global phosphotyrosine survey in triple-negative breast cancer reveals activation of multiple tyrosine kinase signaling pathways. Oncotarget 2015;6: 29143–60.
28. Cerami E, Gao J, Dogrusoz U, Gross BE, Sumer SO, Aksoy BA, et al. The cBio cancer genomics portal: an open platform for exploring multidimensional cancer genomics data. Cancer Discov 2012;2:401–4.
29. Gao J, Aksoy BA, Dogrusoz U, Dresdner G, Gross B, Sumer SO, et al. Integrative analysis of complex cancer genomics and clinical profiles using the cBioPortal. Sci Signal 2013;6:pl1.
30. Ekyalongo RC, Mukohara T, Funakoshi Y, Tomioka H, Kataoka Y, Shimono Y, et al. TYRO3 as a potential therapeutic target in breast cancer. Anticancer Res 2014;34:3337–45.
31. Xu Y, Benlimame N, Su J, He Q, Alaoui-Jamali MA. Regulation of focal adhesion turnover by ErbB signalling in invasive breast cancer cells. Br J Cancer 2009;100:633–43.
32. Guadamillas MC, Cerezo A, Del Pozo MA. Overcoming anoikis–pathways to anchorage-independent growth in cancer. J Cell Sci 2011;124:3189–97.
33. Al-Hajj M, Wicha MS, Benito-Hernandez A, Morrison SJ, Clarke MF. Prospective identification of tumorigenic breast cancer cells. Proc Natl Acad Sci U S A 2003;100:3983–8.
34. Ginestier C, Hur MH, Charafe-Jauffret E, Monville F, Dutcher J, Brown M, et al. ALDH1 is a marker of normal and malignant human mammary stem cells and a predictor of poor clinical outcome. Cell Stem Cell 2007;1:555–67.
35. Maugeri-Sacca M, De Maria R. Hippo pathway and breast cancer stem cells. Crit Rev Oncol Hematol 2016;99:115–22.
36. Moroishi T, Hansen CG, Guan KL. The emerging roles of YAP and TAZ in cancer. Nat Rev Cancer 2015;15:73–9.
37. Lamar JM, Stern P, Liu H, Schindler JW, Jiang ZG, Hynes RO. The Hippo pathway target, YAP, promotes metastasis through its TEAD-interaction domain. Proc Natl Acad Sci U S A 2012;109:E2441–50.
38. Park HW, Guan KL. Regulation of the Hippo pathway and implications for anticancer drug development. Trends Pharmacol Sci 2013;34:581–9.
39. Zhao B, Li L, Tumaneng K, Wang CY, Guan KL. A coordinated phosphorylation by Lats and CK1 regulates YAP stability through SCF(beta-TRCP). Genes Dev 2010;24:72–85.
40. Moroishi T, Park HW, Qin B, Chen Q, Meng Z, Plouffe SW, et al. A YAP/TAZ-induced feedback mechanism regulates Hippo pathway homeostasis. Genes Dev 2015;29:1271–84.
41. Liu-Chittenden Y, Huang B, Shim JS, Chen Q, Lee SJ, Anders RA, et al. Genetic and pharmacological disruption of the TEAD-YAP complex suppresses the oncogenic activity of YAP. Genes Dev 2012;26:1300–5.
42. Wang YH, Israelsen WJ, Lee D, Yu VW, Jeanson NT, Clish CB, et al. Cell-state-specific metabolic dependency in hematopoiesis and leukemogenesis. Cell 2014;158:1309–23.
43. Overholtzer M, Zhang J, Smolen GA, Muir B, Li W, Sgroi DC, et al. Transforming properties of YAP, a candidate oncogene on the chromosome 11q22 amplicon. Proc Natl Acad Sci U S A 2006;103:12405–10.
44. Zhao B, Wei X, Li W, Udan RS, Yang Q, Kim J, et al. Inactivation of YAP oncoprotein by the Hippo pathway is involved in cell contact inhibition and tissue growth control. Genes Dev 2007;21:2747–61.
45. Valent P, Bonnet D, De Maria R, Lapidot T, Copland M, Melo JV, et al. Cancer stem cell definitions and terminology: the devil is in the details. Nat Rev Cancer 2012;12:767–75.
46. Ramos EK, Hoffmann AD, Gerson SL, Liu H. New opportunities and challenges to defeat cancer stem cells. Trends Cancer 2017;3:780–96.
47. Kreso A, Dick JE. Evolution of the cancer stem cell model. Cell Stem Cell 2014;14:275–91.
48. Battula VL, Shi Y, Evans KW, Wang RY, Spaeth EL, Jacamo RO, et al. Ganglioside GD2 identifies breast cancer stem cells and promotes tumorigenesis. J Clin Invest 2012;122:2066–78.
49. Klopp AH, Lacerda L, Gupta A, Debeb BG, Solley T, Li L, et al. Mesenchymal stem cells promote mammosphere formation and decrease E-cadherin in normal and malignant breast cells. PLoS One 2010;5:e12180.
50. Anastasiou D, Yu Y, Israelsen WJ, Jiang JK, Boxer MB, Hong BS, et al. Pyruvate kinase M2 activators promote tetramer formation and suppress tumorigenesis. Nat Chem Biol 2012;8:839–47.

Published OnlineFirst February 12, 2018; DOI: 10.1158/0008-5472.CAN-17-2726

Cancer Research
The Journal of Cancer Research (1916–1930) | The American Journal of Cancer (1931–1940)

AACR American Association for Cancer Research

Oncogenic Kinase–Induced PKM2 Tyrosine 105 Phosphorylation Converts Nononcogenic PKM2 to a Tumor Promoter and Induces Cancer Stem–like Cells

Zhifen Zhou, Min Li, Lin Zhang, et al.

Cancer Res 2018;78:2248-2261. Published OnlineFirst February 12, 2018.